RSC Advances

PAPER

View Article Online
View Journal | View Issue

Cite this: *RSC Adv.*, 2018, **8**, 14328

Photocatalytic degradation of ethylene by Ga_2O_3 polymorphs

Hongshuai Liu,[a] Zeyan Wang,*[a] Huiliang Li,[a] Xiaoyang Zhang,[a] Xiaoyan Qin,[a] Ying Dai,[b] Peng Wang,[a] Yuanyuan Liu[a] and Baibiao Huang*[a]

In this work, we fabricated four different Ga_2O_3 polymorphs, namely, α-, β-, γ-, δ-Ga_2O_3, and investigated their photocatalytic activities by the degradation of ethylene under ultraviolet (UV) light irradiation. Owing to the more positive valence band, all these Ga_2O_3 polymorphs are more photocatalytic reactive than P25 during the degradation of ethylene. The normalized photocatalytic ethylene degradation rate constants of the as-prepared Ga_2O_3 polymorphs follow the order: α-Ga_2O_3 > β-Ga_2O_3 > γ-Ga_2O_3 > δ-Ga_2O_3, which is mainly determined by the position of VBM and the crystallinity of the samples. Among these Ga_2O_3 polymorphs, γ-Ga_2O_3, with the highest surface area, exhibits the highest activity during photocatalytic ethylene degradation, and the degradation rate constant is almost 10 times as that of P25. Furthermore, with the most positive CBM, γ-Ga_2O_3 produces the least CO. These attributes are beneficial for ethylene degradation during post-harvest storage of fruits and vegetables, which makes γ-Ga_2O_3 a potential candidate for practical photocatalytic ethylene degradations.

Received 13th March 2018
Accepted 5th April 2018

DOI: 10.1039/c8ra02212g

rsc.li/rsc-advances

1. Introduction

Ethylene is a colorless and odorless gas that can be produced naturally by plant tissues and biomass fermentation. As ethylene can greatly accelerate the ripening process of fruits and vegetables, serious problems would be encountered during the postharvest storage of fruits and vegetables such as over-ripening, senescence, stimulated chlorophyll loss or promoted abscission of leaves and flowers, *etc.*[1,2] Therefore, it is important to prevent the ethylene action during postharvest storage of fruits and vegetables. Up to now, various methods have been developed to control the action of ethylene such as the use of strong oxidizing agents to decompose ethylene, employing carbon or zeolites as ethylene absorber, or the use of ethylene inhibitor to prevent the synthesis of ethylene, *etc.*[3–7] However, these techniques are usually expensive and require either long exposure times or complicated systems.

Photocatalysis is a potential technique that can utilize solar energy to decompose organic pollutants or generate H_2 by water splitting. Recently, it also emerges as a promising route to prevent ethylene action during the postharvest storage of fruit and vegetables owing to its low cost and continuity.[8–12] For example, Amodio *et al.* demonstrated the completely elimination of ethylene (100 ppm) over TiO_2/SiO_2 composites under UV light irradiation for 2 h. However, comparing to traditional technique, *i.e.*, potassium permanganate based formulation, the photocatalytic degradation rate is still lower.[11] Therefore, it is still needed to further improve the photocatalytic ethylene degradation activity for practical applications.

Up to now, most studies on photocatalytic ethylene degradations are mainly based on the use of TiO_2 as photocatalyst. As the photocatalytic activity on decomposing organic pollutants are mainly determined by the position of the conduction and valence bands of semiconductors, photocatalysts with wider band gaps, such as Ga_2O_3, ZrO_2, are expected to be more efficient than TiO_2. Among these wide band gap semiconductors, Ga_2O_3 is regarded as one of the most promising semiconductors owing to its superior physical and chemical properties and a wide band gap 4.2–5.0 eV, which has been widely investigated on overall water splitting, benzene decomposition and CO_2 reduction, *etc.*[13–17] Therefore, Ga_2O_3 is expected to be more efficient than TiO_2 on photocatalytic ethylene degradations. Moreover, Ga_2O_3 has four polymorphs, namely, α-, β-, γ-, δ-, and ε-Ga_2O_3, which could lead to the variations on photocatalytic activities. For example, Hou *et al.* systematically investigated the photocatalytic activity of Ga_2O_3 polymorphs by decomposing volatile organic compounds, *i.e.*, benzene, toluene, and ethylbenzene. And β-Ga_2O_3 is found to be the most efficient among the Ga_2O_3 polymorphs, which is more than 3 times higher than that of TiO_2.[18] However, the investigations on the photocatalytic ethylene degradations over Ga_2O_3 polymorphs have not been systematically investigated yet.

In this work, we fabricated four Ga_2O_3 polymorphs, namely, α-, β-, γ-, and δ-Ga_2O_3, and investigated their photocatalytic activities on ethylene degradation. The normalized photocatalytic degradation rate constant of the as-prepared Ga_2O_3

[a]State Key Laboratory of Crystal Materials, Shandong University, 250100, P. R. China. E-mail: wangzeyan@sdu.edu.cn; bbhuang@sdu.edu.cn
[b]School of Physics, Shandong University, 250100, P. R. China

polymorphs is found to follow the order of α-Ga_2O_3 > β-Ga_2O_3 > γ-Ga_2O_3 > δ-Ga_2O_3, which is mainly determined by the position of VBM and the crystallinity of the samples. Owing to the highest surface area, γ-Ga_2O_3 exhibits the highest apparent photocatalytic activity on oxidizing ethylene to CO_2, which makes it a potential candidate for practical photocatalytic ethylene degradations.

2. Experimental details

2.1 The fabrication of Ga_2O_3 polymorphs

The Ga_2O_3 polymorphs were fabricated by following the procedures reported elsewhere.[19–21] α- and β-Ga_2O_3 were prepared by calcining GaO(OH) precursors at different temperatures according to literature.[19] In details, 3 g of gallium nitrate hydrate was firstly dissolved in 40 ml ethanol (50 vol%). And then, the solution was slowly added into the aqueous ammonia with the same volume with continuous stirring. After stirring for 1 h at room temperature, the precipitates were filtered and washed with ethanol and deionized water, which was subsequently dried at 60 °C overnight. α- and β-Ga_2O_3 were obtained by calcining the above precursors at 400 and 800 °C for 4 h, respectively. γ-Ga_2O_3 was prepared as follows: 3 g nitrate hydrate was dissolved in 50 ml ethanol solvents, concentrated aqueous ammonia diluted in ethanol (50 vol%) was slowly added under continuous stirring at room temperature until no further precipitate was observed to form. The resulting gel was filtered, thoroughly washed with distilled and ethanol, and vacuum-dried in a desiccator. After that, the metal oxide obtained after it was calcined at 500 °C for 1 hour.[20,21] δ-Ga_2O_3 was prepared by directly calcining gallium nitrate hydrate at 320 °C for 12 hours as reported.[22]

2.2 Characterizations

The XRD patterns of the as-prepared Ga_2O_3 polymorphs were characterized on a Bruker D8 advanced X-ray diffractometer with Cu kα radiation (λ = 1.5418 Å). The morphologies of the Ga_2O_3 polymorphs were obtained by scanning electron microscopy (SEM, Hitachi S-4800), and high-resolution electron transmission electron microscopy (HR-TEM, JEM 2100). The BET surface areas were determined by using N_2 adsorption/desorption isotherm measurements by a Micromeritics ASAP 2020 apparatus. The UV-vis diffuse reflectance spectroscopy (DRS) measurements were recorded on a Shimadzu UV 2550 spectrophotometer equipped with an integrating sphere. X-ray photoelectron spectroscopy (XPS) valence band spectra were measured in a VG Micro-Tech ESCA 3000 X-ray photoelectron spectroscope within monochromatic Al Kα radiation, the photo energy is 1486.6 eV at the condition of >1 × 10^{-9} torr.

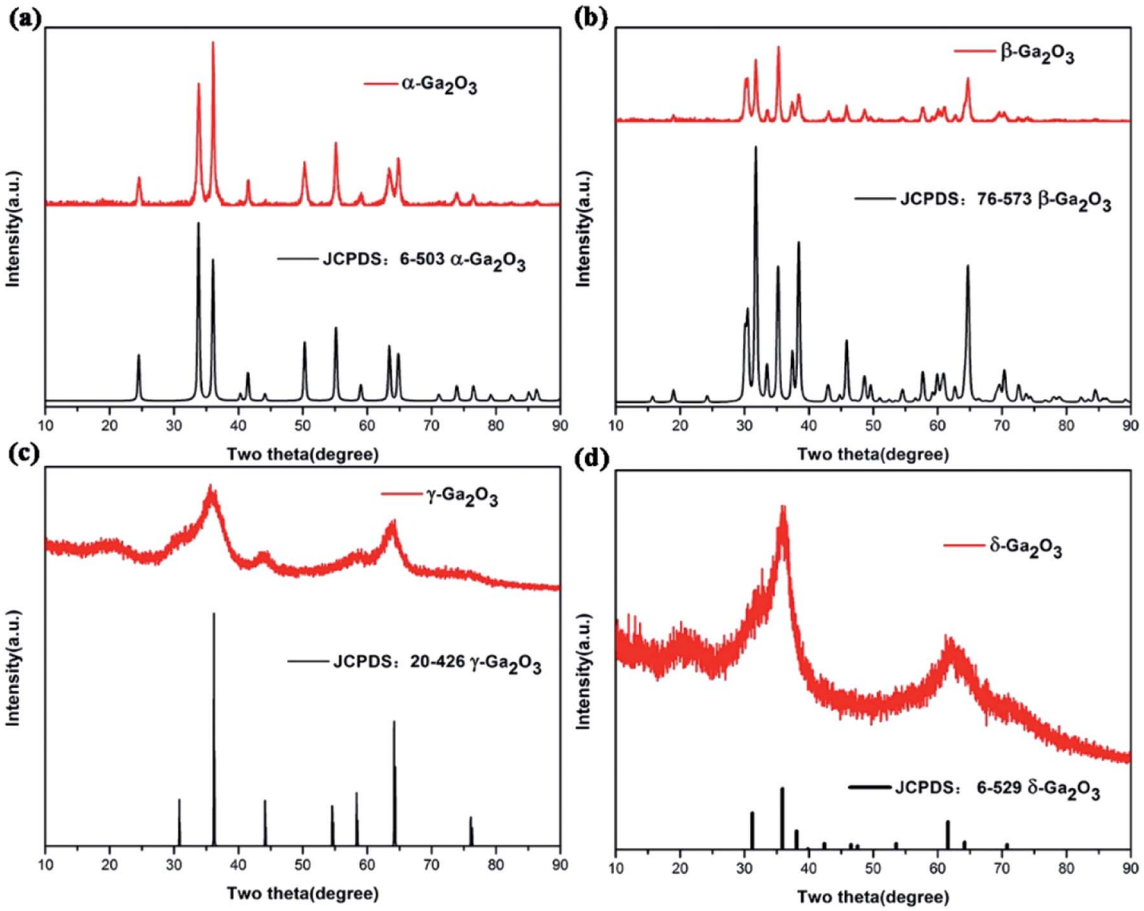

Fig. 1 The XRD patterns of as-prepared Ga_2O_3 polymorphs: (a) α-Ga_2O_3, (b) β-Ga_2O_3, (c) γ-Ga_2O_3, (d) δ-Ga_2O_3, respectively.

2.3 Photocatalytic experiments

The photocatalytic experiments were performed in a closed quartz reactor with a total volume of 420 ml under UV light irradiation (UV lamp, 30 W, 185 nm and 254 nm). Firstly, 0.3 g as-prepared Ga_2O_3 polymorph samples were spread uniformly at the bottom of the reactor. Then, 0.5 ml C_2H_4 was injected into the sealed quartz reactor by a micro-syringe. The quartz reactor was subsequently kept in dark under magnetic stirring for 2 h to reach adsorption–desorption equilibrium before turning on the UV lamp. The reaction temperature was kept at 5 °C by water cooling during the whole experiment. The humidity in the photocatalytic process was 10%. Finally, the quartz reactor was exposed to UV light irradiation for photocatalytic reactions. 30 μl gas was withdrawn from the reactor at 1 h intervals to analyze the concentration of ethylene and carbon dioxide by injection into a gas chromatograph (Shimadzu GC-2014C and GCMS-QP2010 Ultra) equipped with a thermal conductive detector (TCD) and a flame ionization detector (FID). The degradation percentage of ethylene was represented in terms of C/C_0, where C is the concentration of remained ethylene at a certain time, and C_0 is the initial concentration of ethylene injected.

3. Result and discussion

Fig. 1 shows the XRD patterns of as-prepared Ga_2O_3 polymorphs. As shown in this figure, all the XRD peaks of as-prepared samples can be well identified to the characteristic reflections of α-Ga_2O_3 (JCPDS no. 6-503), β-Ga_2O_3 (JCPDS no. 76-573), γ-Ga_2O_3 (JCPDS no. 20-426), δ-Ga_2O_3 (JCPDS no. 06-529), respectively. The broad and poor diffraction peaks of both γ-Ga_2O_3 and δ-Ga_2O_3 indicated the low crystallinity of the materials, which are also in accordance with literature.[23–26]

The morphologies of as-prepared Ga_2O_3 polymorphs were shown in Fig. 2. As shown in Fig. 2(a) and (b), the as-prepared α- and β-Ga_2O_3 exhibit similar morphologies, which are brick-like particles consisted of stacked nanosheets with evenly distributed sizes. The length and width (thickness) of the brick-like particles are ~2 and ~1 μm, respectively. Different from α- and β-Ga_2O_3, the as-prepared γ- and δ-Ga_2O_3 exhibit irregular morphologies consisted of some small nanoparticles as shown in Fig. 2(c) and (d).

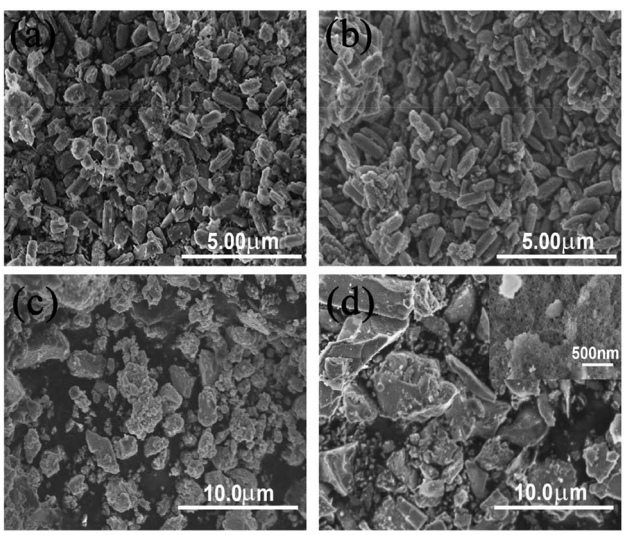

Fig. 2 The morphologies of as-prepared (a) α-Ga_2O_3, (b) β-Ga_2O_3, (c) γ-Ga_2O_3, and (d) δ-Ga_2O_3.

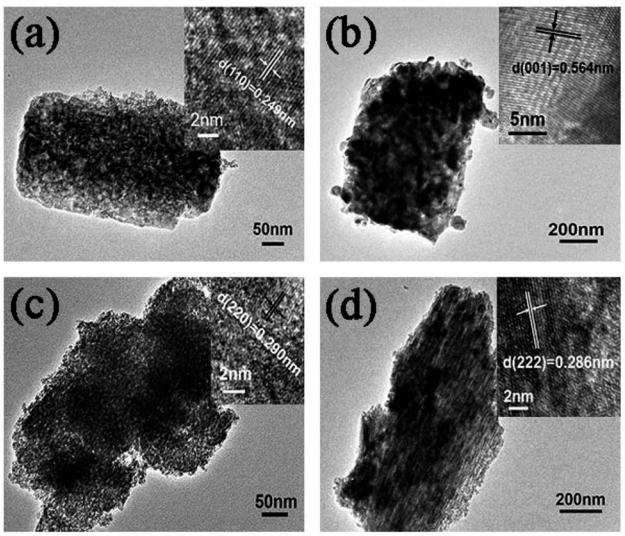

Fig. 3 TEM images of as-prepared (a) α-Ga_2O_3, (b) β-Ga_2O_3, (c) γ-Ga_2O_3, and (d) δ-Ga_2O_3.

For a closer observation, HR-TEM characterizations of the as-prepared Ga_2O_3 polymorphs were carried out as shown in Fig. 3. Although the morphologies of the four Ga_2O_3 polymorphs are different as shown in Fig. 2, all these samples are consisted of some small nanoparticles according to the HR-TEM images as shown in Fig. 3. The clear lattice fringes as shown in the insets of Fig. 3 are corresponding to the (110) plane of α-Ga_2O_3, (001) plane of β-Ga_2O_3, (220) plane of γ-Ga_2O_3, (222) plane of δ-Ga_2O_3, which further confirmed the as-prepared samples are α-, β-, γ-, and δ-Ga_2O_3, respectively. The sizes of the nanoparticles building blocks are quite different, namely, the diameters of the nanoparticle building blocks are 6.6, 19.8, 4.1, and 6.3 nm for α-, β-, γ-, and δ-Ga_2O_3, respectively. And the BET surface areas of the as-prepared Ga_2O_3 polymorphs were also measured as shown in Table 1. The surface areas for α-, β-, γ-, and δ-Ga_2O_3 are 58.45, 17.75, 110.19, and 78.21 $m^2\ g^{-1}$, respectively. This is accordant with the HR-TEM observations, where smaller nanoparticles lead to higher surface areas.

Fig. 4 shows the diffused reflectance spectra of as-prepared Ga_2O_3 polymorphs. As can be seen from this figure, the light

Table 1 Summary of the physicochemical properties of the Ga_2O_3 polymorphs

	α-Ga_2O_3	β-Ga_2O_3	γ-Ga_2O_3	δ-Ga_2O_3
BET surface area ($m^2\ g^{-1}$)	58.45	17.75	110.19	78.21
Band gap (eV)	4.86	4.36	4.43	4.33
Reaction rate constant (h^{-1})	0.661	0.148	0.861	0.217

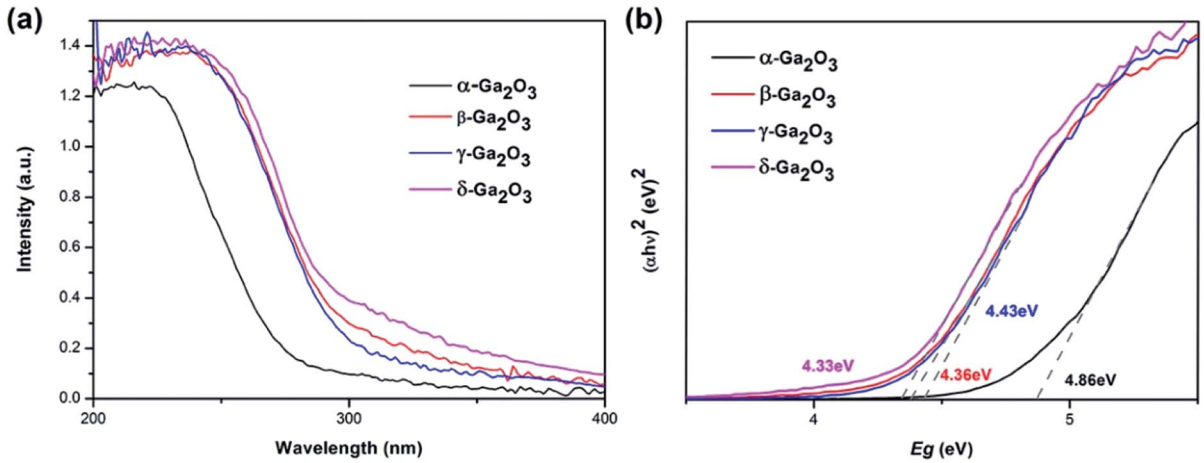

Fig. 4 (a) The diffused reflectance spectra and (b) Tauc's plots of as-prepared α-, β-, γ- and δ-Ga_2O_3.

absorption edge of β-, γ-, and δ-Ga_2O_3 is almost identical, which lies at ~300 nm. But the absorption edge of α-Ga_2O_3 is much shorter, lying at ~270 nm. And as shown in the Tauc's plots of Ga_2O_3 polymorphs in Fig. 4(b), the band gap for α-, β-, γ-, and δ-Ga_2O_3 is calculated to be 4.86, 4.36, 4.33, 4.43 eV, respectively.

The photocatalytic activity of as-prepared Ga_2O_3 polymorphs was evaluated by the degradation of ethylene under UV irradiation. For comparison, P25 was also employed to decompose ethylene under identical condition. As shown in Fig. 5(a), before illumination, dark adsorption experiments were carried out in dark for 2 hours. After the adsorption equilibrium, only a small amount of ethylene was adsorbed by the as-prepared samples. And the ethylene concentrations decrease from 1100 ppm to 1057, 1072, 1096, 1091, 1060 ppm for α-, β-, γ-, δ-

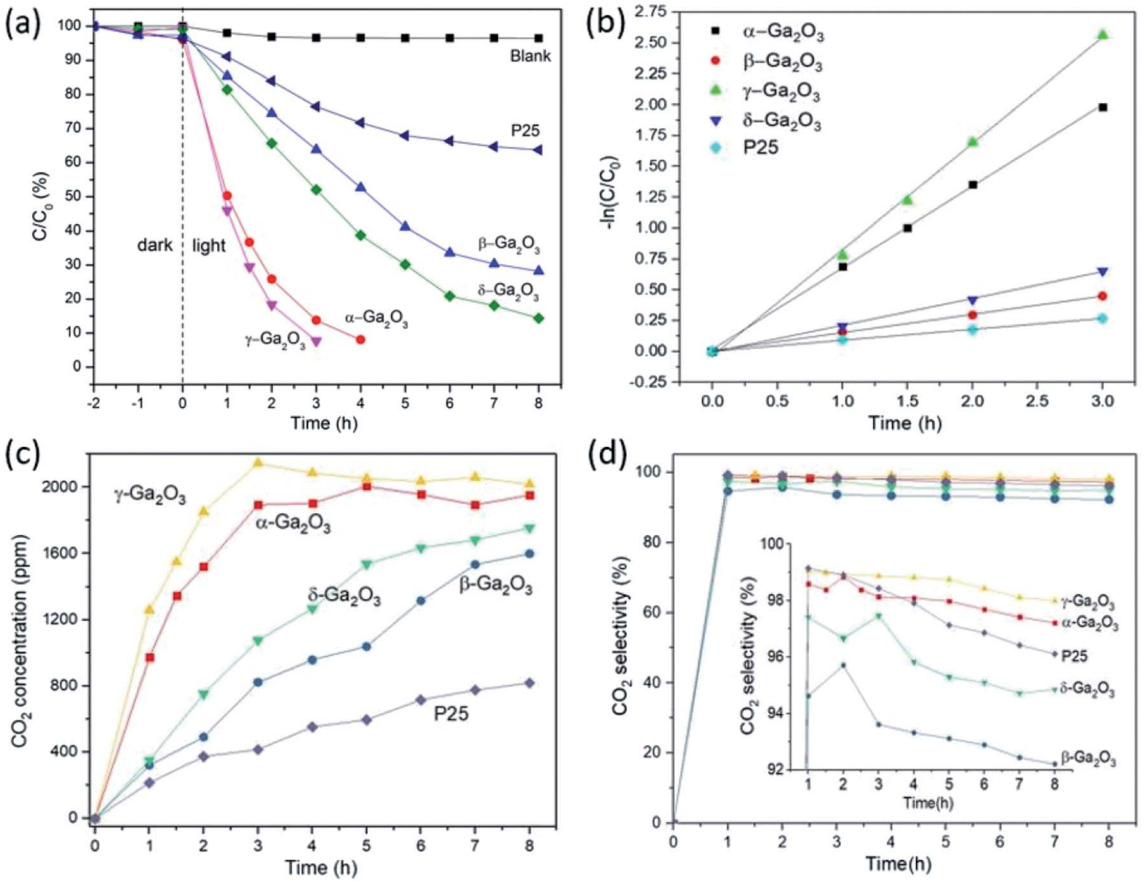

Fig. 5 (a) The photocatalytic ethylene degradation plots and (b) the degradation rate constants over as-prepared Ga_2O_3 polymorphs and P25. (c) The amount of CO_2 produced during the photocatalytic experiments and (d) the percentage of CO_2 in the final products over the as-prepared Ga_2O_3 polymorphs.

Ga_2O_3 and P25, respectively. As shown in the photocatalytic ethylene degradation plots in Fig. 5(a), γ-Ga_2O_3 exhibits the highest photocatalytic activity among these Ga_2O_3 polymorphs, which can decompose the ethylene gas in 3 h. And the photocatalytic activity of α-Ga_2O_3 is slightly lower than that of γ-Ga_2O_3, where the ethylene can be decomposed in 4 h. β- and δ-Ga_2O_3 are less photocatalytic reactive comparing to γ- and α-Ga_2O_3, which can decompose 72% and 86% after irradiated under UV light for 8 h, respectively. However, all the Ga_2O_3 polymorphs exhibit higher activity than P25, where only ~36% of ethylene can be decomposed over P25 under identical conditions in 8 h. The photocatalytic degradation rates of the Ga_2O_3 polymorphs and P25 were also calculated as shown in Fig. 5(b), which exhibit a pseudo-first-order relationship. The degradation rate constant for α-, β-, γ-, δ-Ga_2O_3 and P25 is 0.661, 0.148, 0.861, 0.217 and 0.089 h^{-1}, respectively (Table 1). Apparently, the highest ethylene degradation rate of γ-Ga_2O_3 is nearly 10 times as high as that of P25. As the activity of the photocatalysts is closely related to their specific surface areas, the highest photocatalytic activity of as-prepared γ-Ga_2O_3 could be mainly ascribed to the largest surface areas among these Ga_2O_3 polymorphs. By normalizing the degradation rate constants to the specific surface areas, α-Ga_2O_3 exhibited the highest photocatalytic activity with the normalized rate constant of 0.01132 m^2 $(g\ h)^{-1}$. While, the normalized constant for β-Ga_2O_3, γ-Ga_2O_3, δ-Ga_2O_3, P25 is 0.00836, 0.00781, 0.00278 and 0.00197 m^2 $(g\ h)^{-1}$, respectively. Thus, the photocatalytic activity of the as-prepared Ga_2O_3 polymorphs after normalizing to the surface areas should follow the order: α-Ga_2O_3 > β-Ga_2O_3 > γ-Ga_2O_3 > δ-Ga_2O_3.

As shown in Fig. 5(c), the concentration of CO_2 increases constantly with the degradation of ethylene. As the CO_2 is mainly produced by the photocatalytic degradation of ethylene, the amount of CO_2 produced over different photocatalysts are mainly determined by the photocatalytic degradation of ethylene and accordant with the degradation rate constants as shown in Fig. 5(a) and Table 1. By analyzing the products during the photocatalytic experiments, CO_2 was found to be the main products as shown in Fig. 5(d), which take part in more than 90% of the final products for all the samples. However, the percentage of CO_2 produced over different Ga_2O_3 polymorphs varies a lot as shown in the inset of Fig. 5(d). In detail, the percentage of CO_2 is the highest in γ-Ga_2O_3, which takes 98% of the final products at the end of the photocatalytic experiments. And the percentage of CO_2 for α-Ga_2O_3, P25, δ-Ga_2O_3 and β-Ga_2O_3 is 97.2, 96.1, 94.8, and 92.2%, respectively. More interestingly, the percentage of CO_2 in the products gradually decreased with the increase of the photocatalytic experiment time. This indicates part of the produced CO_2 could be further converted to other secondary products, such as CO and CH_4, which would be unfavorable for the practical applications during the postharvest storage of fruits and vegetables. From this aspect, γ-Ga_2O_3 with highest photocatalytic ethylene degradation rate and highest CO_2 conversion efficiency could be the most suitable candidate among the as-prepared Ga_2O_3 polymorphs for photocatalytic ethylene degradation.

To evaluate the cycling stability of γ-Ga_2O_3, four consecutive-cycle ethylene degradation experiments were conducted. As shown in Fig. 6, the sample does not show any particular loss of photocatalytic activity for ethylene degradation during the repeated experiments. Therefore, γ-Ga_2O_3 can work as an effective photocatalyst for ethylene degradation with good stability.

To probe the mechanism for the different photocatalytic performances of the as-prepared Ga_2O_3 polymorphs, the band structures were investigated by XPS valence spectra. As shown in Fig. 7(a), the valence band maximum (VBM) of the as-prepared Ga_2O_3 polymorphs were determined by extrapolating a linear fit of the low binding energy edge of the valence band spectra to line fitted to the instrument background. The VBM of as-prepared Ga_2O_3 polymorphs can be determined according to the formula:

$$E_{VB} = E + \varphi_{Al} - 4.5$$

where E_{VB} is the position of VBM *vs.* reversible hydrogen electrode (RHE), E is the position of VBM obtained from XPS valence spectra *vs.* the aluminum holder, φ_{Al} is the work function of aluminum (4.2 eV *vs.* vacuum level).[27] The calculated VBM for α-, β-, γ-, and δ-Ga_2O_3 lies at 3.54, 2.87, 3.04, and 2.75 eV (*vs.* RHE), respectively. Combining the band gaps estimated from the diffused reflectance spectra as shown in Fig. 4(b), the band diagrams for the as-prepared Ga_2O_3 polymorphs can be obtained as shown in Fig. 7(b). According to the calculated band structures of the as-prepared Ga_2O_3 polymorphs, the oxidability of the photogenerated holes for the Ga_2O_3 polymorphs should follow the order: α-Ga_2O_3 > γ-Ga_2O_3 > β-Ga_2O_3 > δ-Ga_2O_3, and the reducibility of the photogenerated electrons follow the order: δ-Ga_2O_3 > β-Ga_2O_3 > α-Ga_2O_3 > γ-Ga_2O_3.

As the photocatalytic ethylene degradation into CO_2 is an oxidation process, the photocatalytic ethylene degradation activity of as-prepared Ga_2O_3 polymorphs is mainly determined by their VBM, and should follow the order: α-Ga_2O_3 > γ-Ga_2O_3 > β-Ga_2O_3 > δ-Ga_2O_3. This order is almost accordant with the

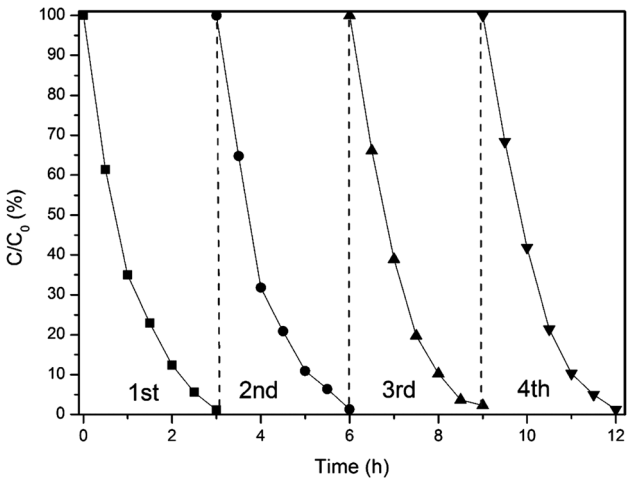

Fig. 6 Four consecutive-cycles of γ-Ga_2O_3 for photocatalytic ethylene degradation.

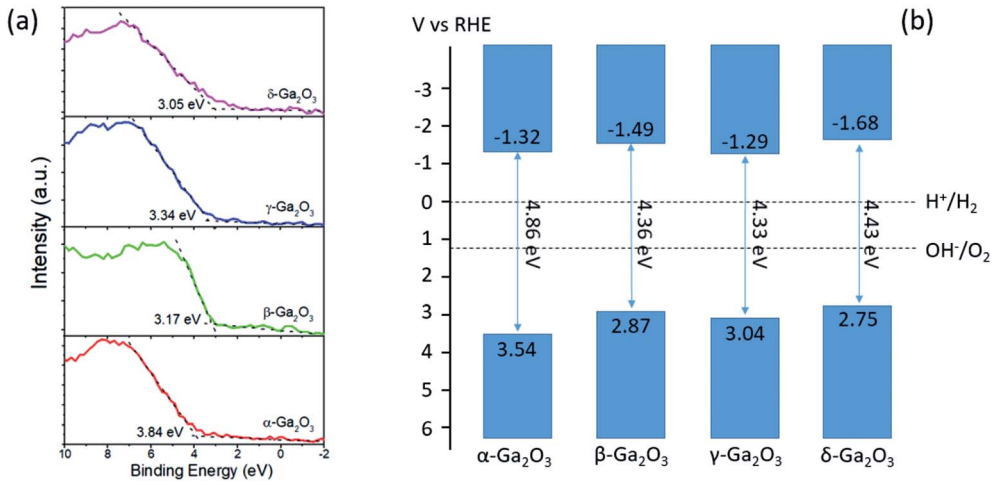

Fig. 7 (a) The XPS valence spectra of as-prepared Ga_2O_3 polymorphs. (b) The calculated band diagrams for α-, β-, γ-, and δ-Ga_2O_3, respectively.

normalized degradation rate constants for the as-prepared Ga_2O_3 polymorphs except for β-Ga_2O_3, where β-Ga_2O_3 with more negative VBM is more reactive than γ-Ga_2O_3. This could be due to the higher crystallinity of β-Ga_2O_3 as evidenced by the sharper XRD diffraction peaks as shown in Fig. 1 than γ-Ga_2O_3, because photogenerated charge carriers recombine more quickly in poorly crystallized photocatalysts. Besides the effects of VBM and crystallinity, the photocatalytic performances of photocatalysts were also closely related to the surface areas of the photocatalysts. Thus, although the normalized degradation rate constant of α- and β-Ga_2O_3 is higher than γ-Ga_2O_3, the overall photocatalytic performance of γ-Ga_2O_3 is the highest among the as-prepared Ga_2O_3 polymorphs owing to the highest specific surface areas. Additionally, with the most positive CBM, γ-Ga_2O_3 produces the least CO during the photocatalytic ethylene degradation among the Ga_2O_3 polymorphs. Both of these attributes are favorable for photocatalytic ethylene degradation during the post-harvest storage of fruits and vegetables, which make γ-Ga_2O_3 a potential candidate for practical photocatalytic ethylene degradations.

4. Conclusions

In this work, we fabricated four Ga_2O_3 polymorphs and investigated their photocatalytic activities on ethylene degradation. According to the experimental results, all the as-prepared Ga_2O_3 polymorphs exhibit higher photocatalytic activities on ethylene degradation than P25 under UV light irradiation. The normalized photocatalytic ethylene degradation rate constant of the as-prepared Ga_2O_3 polymorphs follows the order: α-Ga_2O_3 > β-Ga_2O_3 > γ-Ga_2O_3 > δ-Ga_2O_3, which could be ascribed to the synergistic effects of the VBM position and the crystallinity of the samples. Due to the highest surface area, γ-Ga_2O_3 exhibits the highest photocatalytic activity for ethylene degradation among these Ga_2O_3 polymorphs, which has a degradation rate constant 10 times as high as that of P25. Furthermore, γ-Ga_2O_3 produces the least CO during ethylene degradation due to its more positive CBM. Based on these attributes, γ-Ga_2O_3 is regarded as a potential candidate for photocatalytic ethylene degradations that could be applied in the post-harvest storage of fruits and vegetables.

Conflicts of interest

The authors declare no competing financial interest.

Acknowledgements

This work is financially supported by the National Natural Science Foundation of China (21333006, 21573135, and 51602179), the National Basic Research Program of China (the 973 program, 2013CB632401). B. B. H. acknowledges the support from Taishan Scholars Program of Shandong Province, and Z. Y. W. acknowledges support from Young Scholars Program of Shandong University (2015WLJH35).

References

1 B. Kartheuser and C. Boonaert, *J. Adv. Oxid. Technol.*, 2007, **10**(1), 107–110.
2 M. E. Saltveit, *Postharvest Biol. Technol.*, 1999, **15**(3), 279–292.
3 L. Vermeiren, F. Devlieghere, M. Van Beest, N. De Kruijf and J. Debevere, *Trends Food Sci. Technol.*, 1999, **10**(3), 77–86.
4 G. Capitani, E. Hohenester, L. Feng, P. Storici, J. F. Kirsch and J. N. Jansonius, *J. Mol. Biol.*, 1999, **294**(3), 745–756.
5 D. Martínez-Romero, G. Bailén, M. Serrano, F. Guillén, J. M. Valverde, P. Zapata, S. Castillo and D. Valero, *Crit. Rev. Food Sci. Nutr.*, 2007, **47**(6), 543–560.
6 Z.-X. Liu, J.-N. Park, S. H. R. Abdi, S.-K. Y Park, Y.-K. Park and C. W. Lee, *Top. Catal.*, 2006, **39**(3–4), 221–226.
7 G. Bailén, F. Guillén, S. Castillo, M. Serrano, D. Valero, D. Martínez-Romero and J. Agric, *Food Chem.*, 2006, **54**, 2229–2235.
8 C. Maneerat, Y. Hayata, N. Egashira, K. Sakamoto, Z. Hamai and M. Kuroyanagi, *Trans. ASABE*, 2003, **46**(3), 725–730.

9 S.-Y. Ye, Q.-M. Tian, X.-L. Song and S.-C. Luo, *J. Photochem. Photobiol., A*, 2009, **208**(1), 27–35.
10 M. Hussain, S. Bensaid, F. Geobaldo, G. Saracco and N. Russo, *Ind. Eng. Chem. Res.*, 2011, **50**(5), 2536–2543.
11 M. L. V. De Chiara, S. Pal, A. Licciulli, M. L. Amodio and G. Colelli, *Biosyst. Eng.*, 2015, **132**, 61–70.
12 X. Z. Liang, P. Wang, M. M. Li, Q. Q. Zhang, Z. Y. Wang, Y. Dai, X. Y. Zhang, Y. Y. Liu, M.-H. Whangbo and B. B. Huang, *Appl. Catal., B*, 2018, **220**, 356–361.
13 M. Seijiro, Y. Yutaka and O. koichiro, *Chem. Lett.*, 2004, **33**(3), 294–295.
14 Y. D. Hou, J. J. Zhang, Z. X. Ding and L. Wu, *Powder Technol.*, 2010, **203**(3), 440–446.
15 H. Oveisi, C. Anand, A. Mano, S. S. Al-Deyab, P. Kalita, A. Beitollahi and A. Vinu, *J. Mater. Chem.*, 2010, **20**, 10120–10129.
16 T. F. Liu, L. Tranca, J. X. Yang, X. Zhou and C. Li, *J. Mater. Chem. A*, 2015, **3**, 10309–10319.
17 H. Abdullah, N. S. Gultom and D.-H. Kuo, *New J. Chem.*, 2017, **41**, 12397–12406.
18 Y. D. Hou, L. Wu, X. C. Wang, Z. X. Ding, Z. H. Li and X. Z. Fu, *J. Catal.*, 2007, **250**(1), 12–18.
19 Y. D. Hou, X. C. Wang, L. Wu, Z. X. Ding and X. Z. Fu, *Environ. Sci. Technol.*, 2006, **40**(18), 5799–5803.
20 C. Otero Areán, A. L. Bellan, M. P. Mentruit, M. R. Delgado and G. T. Palomino, *Microporous Mesoporous Mater.*, 2000, **40**(1–3), 35–42.
21 J. Bohm, *Angew. Chem.*, 1940, **53**, 131.
22 R. Roy, V. G. Hill and E. F. Osborn, *J. Am. Chem. Soc.*, 1952, **74**, 719–722.
23 C.-C. Huang and C.-S. Yeh, *New J. Chem.*, 2010, **34**, 103–107.
24 L. D. Li, W. Wei and M. Behrens, *Solid State Sci.*, 2012, **14**, 971–981.
25 M. Zinkevich, F. M. Morales, H. Nitsche, M. Ahrens, M. Rühle and F. Aldinger, *Z. Metallkd.*, 2004, **95**(9), 756–762.
26 M. Hegde, T. Wang, Z. L. Miskovic and P. V. Radovanovic, *Appl. Phys. Lett.*, 2012, **100**(14), 141903–141907.
27 M. T. Greiner, M. G. Helander, W.-M. Tang, Z.-B. Wang, J. Qiu and Z.-H. Lu, *Nat. Chem.*, 2012, **11**, 76–81.